2023 IEEE International Conference on Robotics and Automation (ICRA 2023)
May 29 - June 2, 2023. London, UK

Multi-Modal Learning and Relaxation of Physical Conflict for an Exoskeleton Robot with Proprioceptive Perception

Xuan Zhang, Yana Shu, Yu Chen, Gong Chen, Jing Ye, Xiu Li, and Xiang Li

Abstract— **Exoskeleton robots provide assistive forces to suit the human subject via physical human-robot interaction. During the closely-coupled interaction, a mismatch between the wearer and the robot may result in physical conflict, which could affect assistance efficiency or even compromise safety. Therefore, such conflicts should be accurately detected and then properly relaxed by adjusting the robot's action. This paper proposes a new learning scheme to detect physical conflicts between humans and robots. The constructed learning network receives multi-modal information from proprioceptive sensors and then outputs the anomaly score to specify the physical conflict, which score is further used to continuously adjust the robot impedance to ensure a safe and efficient interaction. Such a formulation allows the robot to explore the semantic information during the interaction (e.g., gait phases, imbalance, human fatigue) and hence react properly to the physical conflict. Experimental results and comparative studies on a lower-limb exoskeleton robot are presented to illustrate that the proposed learning scheme can deal with physical conflicts in a faster and more accurate manner.**

I. Introduction

Exoskeleton robots provide assistive forces to the human subject via the close and intensive coupling between the wearer and the robot. Specifically, the lower-limb exoskeleton robots are used in rehabilitation training [1], to actively help stroke patients to walk, or to simply support the wearer's weight during repetitive and labor-intensive work [2].

However, a mismatch between the wearer and the robot may result in physical conflict, that is, the motions of both parties are not well synchronized [3], or the robot's assistance dose not suit the human's motion intention [4]. It is usually not trivial to accurately and promptly detect such conflicts, due to the varying dynamic model of human limbs or the uncertainty in human motion intention [5], [6]. Failure to detect such conflicts could affect assistance efficiency or even compromise safety. Given that conflicts can be successfully detected, the exoskeleton robot should also properly adjust its behavior to address or relax said conflicts.

In this paper, a new learning scheme is proposed to assess physical conflicts between humans and wearable robots through a detection network; the advantages of which are summarised as follows.

X. Zhang, Y. Shu, and Xiu Li are with the Tsinghua Shenzhen International Graduate School, Tsinghua University, China. Y. Chen and Xiang Li are with the Department of Automation, Tsinghua University, China. G. Chen and J. Ye are with Shenzhen MileBot Robotics Co., Ltd, China. This work was supported in part by the National Natural Science Foundation of China under Grant U21A20517 and 52075290, in part by the Science and Technology Innovation 2030-Key Project under Grant 2021ZD0201404, and in part by Shenzhen Science and Technology Program under Grant KQTD20200909114235003. Corresponding author: Xiang Li (xiangli@tsinghua.edu.cn)

- The proposed scheme is dependent on the proprioceptive sensors of the exoskeleton robot only, (i.e., IMUs, encoders, torque sensors); hence, it is easy to implement and of low cost.
- The constructed detection network explores semantic information (e.g., gait phases, imbalance, human fatigue) by using proprioceptive sensors, thereby improving the accuracy of conflict detection.
- The developed control method is able to continuously modulate robot impedance to relax conflicts, according to the anomaly score from the detection network.

The development of the proposed control scheme follows the approach of singular perturbation, and a disturbance observer is also introduced to eliminate the need for force sensors for impedance control. A series of ablation studies and experiments on a lower-limb exoskeleton robot are carried to illustrate the advantage of multi-modal detection and the effectiveness of the proposed control scheme.

II. Related Works

Anomaly Detection: In general, physical conflicts can be treated as abnormal cases during human-robot interaction. Anomaly detection methods can detect abnormal values in the monitoring data, so as to find abnormal conditions during operation, such as machine failure, operation error and so on. Compared to the model-based method, deep anomaly detection (DAD) technology is able to capture the relationship between multi-modal data and the executing task, thereby learning complex features to deal with large-scale data sets [7].

For robot manipulators coexisting with humans, it is important to avoid collisions to guarantee the safety. To handle the imbalance between the collision data and the normal data, numerous learning-based anomaly detection methods have been proposed. In [8], [9], anomaly data was detected by k-mean clustering algorithms. In [10]–[12], the LOF algorithm was employed to solve the anomaly detection problem. A novel unsupervised approach for anomaly detection based on deep residual autoencoders was proposed in [13].

To detect an abnormal state from the time-series data, Pankaj Malhotra *et al.* referred to a recurrent neural network (RNN) and proposed an LSTM-based anomaly detection method (LSTM-AD) [14]; However, this method does not function for time-series with unpredictable external changes. Daehyung Park *et al.* proposed a multimodal anomaly detector using an LSTM-based variational autoencoder (LSTM-VAE) [15], which can model the underlying probability distribution of observations. In [16], Ya Su *et al.* proposed a

GRU-based multivariate time series anomaly detector, called OmniAnomaly.

Considering that it is usually difficult to describe the model of physical conflicts for exoskeleton robots, this paper also uses a learning technique (specifically, VAE), to detect anomalies using both multi-modal and time-series sensory information.

Variable Impedance Control: Variable impedance control (VIC) for robotic systems is inspired by human behavior and biomechanics, where the central nervous system can continuously modulate the physical impedance of human limbs to adapt to uncertain environments and different types of tasks, to resist external perturbation and so on [17], [18]. In [19], VIC was deployed in a lower-limb rehabilitation exoskeleton, where the deviation between the human intended motion and the current joint angle of the exoskeleton was utilized to vary the impedance parameters to relieve physical conflict. In [20], VIC was applied to a collaborative assembly task, where the robot varied its stiffness based on the interaction with the human subject and the learned impedance behavior from demonstrations. Furthermore, the impedance parameters can also be adjusted by taking into account a range of other variables, such as velocity [21] and the location of the center of mass [22].

Various learning-based approaches, such as the reinforcement learning algorithm, have also been employed to perform impedance variation while dealing with uncertainties. In [23], an inverse-reinforcement-learning-based method was designed for impedance learning, where the reward function associated with the trajectory tracking error and the impedance switching policy for the action space were learned from expert demonstrations. In [24], a policy of reinforcement learning was formulated as a combination of output impedance and desired trajectory, and a reward term was designed to implement the learned variable impedance policy. In [25], the approach of dynamic movement primitives (DMPs) was introduced to learn and reproduce the movement trajectory and stiffness profile learned from demonstrations. In [26], a GMM based state-dependent variable impedance law was designed to transfer human impedance behavior to the robot while ensuring stability.

While much progress has been made in VIC of exoskeleton robots, most of the existing control schemes can not detect then relax the physical conflicts, such as motion asynchronization, human fatigue, and imbalance during walking.

III. Preliminaries

This paper considers the exoskeleton robot driven by series elastic actuators (SEAs), where the principle is illustrated in Fig. 1. Different from rigid actuators, an elastic element (e.g., a spring) is installed between the driving motor and the robot joint, which can store the excessive energy and has the tolerance to impacts.

The dynamic model of a SEA-driven exoskeleton robot

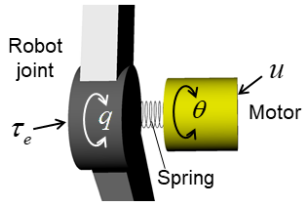

Fig. 1. An illustration of a robot joint driven by SEA, where the spring is installed between the driving motor and the robot joint. Specifically, $\boldsymbol{u}$ is the control input exerted by the motor, $\boldsymbol{\tau}_e$ denotes the interaction torque, $\boldsymbol{q}$ is the rotational angle of the robot joint, and $\boldsymbol{\theta}$ denotes the rotation of motor rotor.

can be described as:

$$\boldsymbol{M}(\boldsymbol{q})\ddot{\boldsymbol{q}} + \boldsymbol{C}(\dot{\boldsymbol{q}}, \boldsymbol{q})\dot{\boldsymbol{q}} + \boldsymbol{g}(\boldsymbol{q}) = \boldsymbol{K}(\boldsymbol{\theta} - \boldsymbol{q}) + \boldsymbol{\tau}_e, \quad (1)$$

$$\boldsymbol{B}\ddot{\boldsymbol{\theta}} + \boldsymbol{K}(\boldsymbol{\theta} - \boldsymbol{q}) = \boldsymbol{u}, \quad (2)$$

where (1) describes the subsystem at the robot side, (2) describes the subsystem at the actuator side, and both subsystems are coupled with the output torque of the SEA, that is, $\boldsymbol{K}(\boldsymbol{\theta}-\boldsymbol{q})$. Specifically, $\boldsymbol{q} \in \Re^n$ denotes the vector of the joint angles of the robot, n is the number of DoFs, $\boldsymbol{\theta} \in \Re^n$ denotes the vector of the rotational angles of the rotors, $\boldsymbol{K} \in \Re^{n\times n}$ is the stiffness matrix, $\boldsymbol{M}(\boldsymbol{q}), \boldsymbol{B} \in \Re^{n\times n}$ are the inertia and damp matrices for the robot and the actuator respectively, $\boldsymbol{C}(\dot{\boldsymbol{q}}, \boldsymbol{q}) \in \Re^{n\times n}$ is a matrix related to the Centripetal and Coriolis forces, $\boldsymbol{g}(\boldsymbol{q}) \in \Re^n$ is a vector of gravitational torque, $\boldsymbol{\tau}_e \in \Re^n$ is a vector related to physical interaction, and $\boldsymbol{u} \in \Re^n$ denotes the control input, which is also the torque exerted by the driving motor.

Some properties of the dynamic model described by (1) and (2) are listed as follows [27], [28]

1) The matrix $\boldsymbol{M}(\boldsymbol{q})$ is bounded, symmetric, and positive definite;
2) The term $\dot{\boldsymbol{M}}(\boldsymbol{q}) - 2\boldsymbol{C}(\boldsymbol{q}, \dot{\boldsymbol{q}})$ is skew-symmetric;
3) The matrices $\boldsymbol{B}$ and $\boldsymbol{K}$ are constant, diagonal, and positive definite.

This paper is to develop a model-based control scheme for the exoskeleton robot, where the dynamic parameters (i.e., $\boldsymbol{M}(\boldsymbol{q})$, $\boldsymbol{C}(\dot{\boldsymbol{q}}, \boldsymbol{q})$, $\boldsymbol{g}(\boldsymbol{q})$, $\boldsymbol{K}$, $\boldsymbol{B}$) are assumed to be known, which can be obtained with sufficient accuracy by using the identification technique [29].

IV. Multi-Modal Detection Network

The conflict-detection network is constructed by referring to the variational autoencoders (VAEs) [15] and its structure is shown in Fig. 2. It can be considered as a real-time semi-supervised anomaly detector that receives multi-modal sensory information, namely:

- *IMUs* - to identify the gait phases;
- *Torques* - to measure the physical interaction between human and robot;
- *Encoders* - to assess the synchronization between human and robot.

The use of the multi-modal information helps the robot better understand and detect the physical conflicts at the semantic

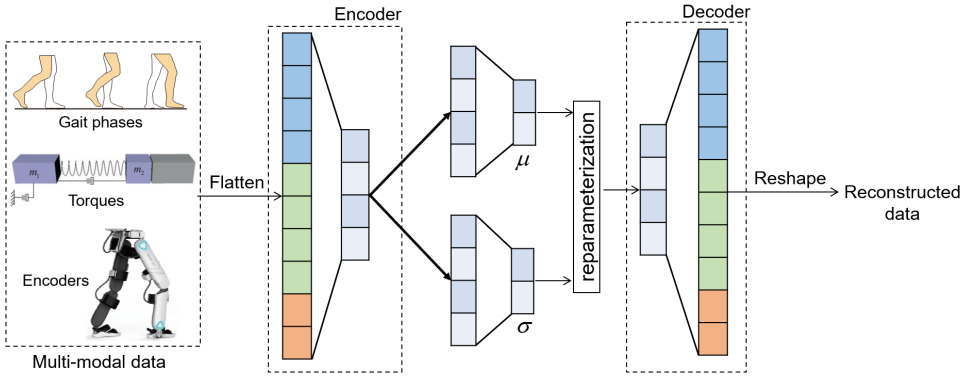

Fig. 2. Structure of the detection network, which receives the multi-modal information from proprioceptive sensors then generates the anomaly score.

level. Since all the information is obtained with proprioceptive sensors, the proposed scheme is easy to implement and of low cost.

To handle the time-series signals, the sliding window is introduced to represent the segment of data and then fed into the network. In addition, both the encoder and the decoder are composed of two fully-connected layers activated by rectified linear unit (ReLu), where the first fully-connected layer of encoder acts as the equivalent to a flatten layer. The aforementioned has been summarized in Table I.

TABLE I
THE ARCHITECTURE OF THE DETECTION NETWORK

Layer	Input size	Output size
Flatten	(100,10)	(1000,1)
FC[1]	(1000,1)	(400,1)
FC (μ, σ)[2]	(400,1)	(50,1)
FC	(50, 1)	(400,1)
FC	(400, 1)	(1000,1)
Reshape	(1000,1)	(100,10)

[1] FC denotes fully-connected layer.
[2] μ and σ are mean and variance of the latent variables respectively.

In the proposed network, latent variables are utilized to capture normal patterns of the input signals and then to reconstruct the original data; The anomaly score is obtained by calculating the reconstruction error, which increases when the physical conflict is more significant and decreases when the conflict is relaxed.

To train the proposed network, the latent variable l is reparameterized and given as [30]:

$$l = \mu + \sigma \odot \epsilon, \tag{3}$$

where μ and σ are parameters obtained from the encoder which represent mean and standard deviation, respectively. Sample noise is set to obey standard normal distribution i.e., $\epsilon \sim \mathcal{N}(0, \boldsymbol{I})$.

Next, the loss function is formulated as

$$\mathcal{L}_{train}(\mathbf{x}^t) = ||\mathbf{x}^t - \hat{\mathbf{x}}^t||^2 + KL[\mathcal{N}(\mu, \sigma), \mathcal{N}(0, \boldsymbol{I})], \tag{4}$$

which comprises both the reconstruction error and the KL-divergence, where $\hat{\mathbf{x}}^t$ denotes the output of the decoder.

Then, the anomaly score can be defined as

$$s = MSE(\mathbf{x}^t, \hat{\mathbf{x}}^t)/100 = ||\mathbf{x}^t - \hat{\mathbf{x}}^t||^2/100 \tag{5}$$

The exoskeleton robot refers to the anomaly score to adjust its assistance and hence relaxes physical conflicts with the wearer. The adjustment should fulfill the following requirements.

- When the anomaly score oscillates around a small value, the robot should ignore such minor conflicts to avoid over-reaction;
- When the anomaly score exceeds a certain threshold, significant conflicts may arise, such that the robot should quickly react to address it.

To achieve it, the anomaly score is mapped into a weighting function as

$$w(s) = \lambda_1 \tanh(-\tfrac{s}{m} + h) + \lambda_2 \tag{6}$$

where λ_1 and λ_2 are two positive constants determine the range and middle of weighting function, m is a constant to normalize the anomaly score into a specified small range, h represents the offset of weighting function from the origin of coordinates along horizontal axis's positive direction. An example of the weighting function is shown in Fig. 3.

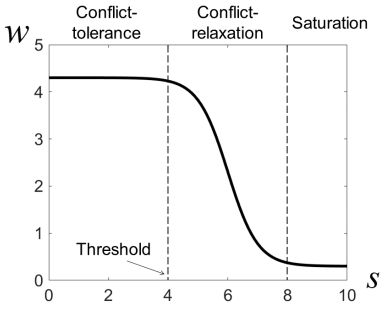

Fig. 3. An example of the weighting function, whose variation is to modulate the robot's impedance. Specifically, λ_1=2, λ_2=2.3, m=1, h=6. Note that the length of "conflict-relaxation" zone is given as $4 < s < 8$, where the robot is to lower its output impedance to become passive; When $s > 8$, the weighting function is saturated to maintain the minimal assistance.

V. Variable Impedance Control with Conflict Relaxation

In this section, a variable impedance model is proposed for the exoskeleton robot to regulate its action in the presence of physical conflict between the human and the robot.

First, the desired impedance model is described as

$$\boldsymbol{C}_d(\dot{\boldsymbol{q}} - \dot{\boldsymbol{q}}_d) + \boldsymbol{K}_d(\boldsymbol{q} - \boldsymbol{q}_d) = \tfrac{1}{w(s)}\boldsymbol{\tau}_e, \tag{7}$$

where $\boldsymbol{q}_d \in \Re^n$ is the reference trajectory in joint space, $\boldsymbol{C}_d, \boldsymbol{K}_d \in \Re^{n\times n}$ represent the parameters of the desired damping and stiffness in the desired impedance model, respectively. Note that (7) describes a first-order system, where the desired inertia is not included. Such an impedance model matches the lower-limb model of human subject [31].

Multiplying both sides of (7) with $w(s)$, the desired impedance model can be expressed as

$$\boldsymbol{C}_d(t)(\dot{\boldsymbol{q}} - \dot{\boldsymbol{q}}_d) + \boldsymbol{K}_d(t)(\boldsymbol{q} - \boldsymbol{q}_d) = \boldsymbol{\tau}_e, \tag{8}$$

where $\boldsymbol{C}_d(t) \triangleq w(s)\boldsymbol{C}_d$ and $\boldsymbol{K}_d(t) \triangleq w(s)\boldsymbol{K}_d$, varying according to the weighting function. Specifically, when the anomaly score increases and enters the "conflict-relaxation" zone, $w(s)$ is scaled down, thus lowering the impedance parameters and hence driving the robot to become more passive to relax the conflict. Otherwise, the impedance parameters return to their original values to maintain the assistance.

Then, an impedance vector is introduced as

$$\begin{aligned}\boldsymbol{z} &= \dot{\boldsymbol{q}} - \dot{\boldsymbol{q}}_r \\ &= \dot{\boldsymbol{q}} - \dot{\boldsymbol{q}}_d + \boldsymbol{C}_d^{-1}\boldsymbol{K}_d(\boldsymbol{q} - \boldsymbol{q}_d) - \tfrac{1}{w(s)}\boldsymbol{C}_d^{-1}\boldsymbol{\tau}_e,\end{aligned} \tag{9}$$

where

$$\dot{\boldsymbol{q}}_r = \dot{\boldsymbol{q}}_d - \boldsymbol{C}_d^{-1}\boldsymbol{K}_d(\boldsymbol{q} - \boldsymbol{q}_d) + \tfrac{1}{w(s)}\boldsymbol{C}_d^{-1}\boldsymbol{\tau}_e \tag{10}$$

is a reference vector. From (9), it can be found that the convergence of $\boldsymbol{z} \to \boldsymbol{0}$ implies the realization of the desired impedance model (7).

Note that the impedance vector (9) is dependent on the interaction torque $\boldsymbol{\tau}_e$. To eliminate the need to use sensors for torque measurement, a model-based observer is proposed to estimate the interaction torque as $\hat{\boldsymbol{\tau}}_e$ [32]. It can be proved that the observer ensures the convergence of $\hat{\boldsymbol{\tau}}_e \to \boldsymbol{\tau}_e$, and using the estimated interaction torque in the impedance vector (9) can eliminate the need for torque sensors.

The development of the proposed impedance control scheme follows the approach of singular perturbation [33], because the overall dynamic model, described by (1) and (2), exhibits different time scales and can be modeled as a "fast-slow" system. That is, the control input is given as

$$\boldsymbol{u} = \boldsymbol{u}_s + \boldsymbol{u}_f, \tag{11}$$

where $\boldsymbol{u}_s$ and $\boldsymbol{u}_f$ represents the slow and the fast time-scale control terms, respectively.

Specifically, the fast time-scale control term, stabilizing (2), is designed as

$$\boldsymbol{u}_f = -\boldsymbol{K}_v(\dot{\boldsymbol{\theta}} - \dot{\boldsymbol{q}}), \tag{12}$$

where $\boldsymbol{K}_v \in \Re^{n\times n}$ is a diagonal and positive-definite matrix.

Next, using the estimated interaction torque $\hat{\boldsymbol{\tau}}_e$, the slow time-scale control term is proposed to stabilize (1) and achieve the desired impedance model as

$$\begin{aligned}\boldsymbol{u}_s = &-\boldsymbol{K}_z\boldsymbol{z} - \hat{\boldsymbol{\tau}}_e \\ &+(\boldsymbol{M}(\boldsymbol{q}) + \boldsymbol{B})\ddot{\boldsymbol{q}}_r + \boldsymbol{C}(\dot{\boldsymbol{q}}, \boldsymbol{q})\dot{\boldsymbol{q}}_r + \boldsymbol{g}(\boldsymbol{q}),\end{aligned} \tag{13}$$

where $\boldsymbol{K}_z \in \Re^{n\times n}$ is a diagonal and positive-definite matrix.

It can be proved that the proposed control scheme, described by (11), (12), and (13), guarantees the stability of closed-loop system and also the convergence of the impedance vector to zero. Hence, the proposed variable impedance model (7) is realized. The details of the proof are given in the appendix.

VI. Experiment

A. Experimental Setup

The proposed scheme was implemented in a bilateral lower-limb exoskeleton robot to validate its performance, as shown in Fig. 4. All the four joints of the robot (that is, two hip joints and two knee joints) are driven with SEAs, where the spring stiffness of SEA is given as $635\ Nm$, and the output torque of SEA can be computed with the spring deflection (measured by encoders) and the known stiffness. The robot is mainly equipped with two types of proprioceptive sensors, that is, inertial measurement units (IMUs, JY901) and encoders (2048 lines). The proprioceptive sensors can be used to measure all the aforementioned multi-modal information, including the gait phases (with IMUs), interaction torque (with encoders), and relative motion between the human and the robot (with IMUs and encoders). During the experiment, four wireless surface electromyographic sensors (Ws450, biometrics Ltd.) are mounted on human leg muscles, namely the quadriceps femoris (QF) and tibialis anterior muscle (TA) of the left and right legs, to collect the feedback of human limb and hence assess the performance of the proposed controller.

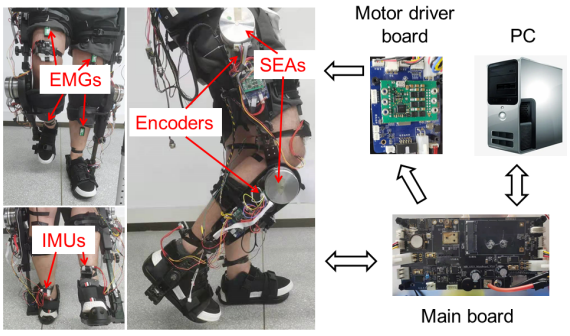

Fig. 4. Experimental setup of the exoskeleton robot, where all four joints of both legs are driven by the SEAs. The main board, combined with the PC, realized the detection network and the control algorithm then sent the commands to the four slave boards to drive the robot joints respectively.

An embedded main board is set to communicate with the PC shown in Fig. 4, where the detection network runs on the PC and the control algorithm is programmed and realized by the main board. The main board sends the control commands via the pulse width modulation (PWM) signals to the four

slave boards to drive the motion of the four robot joints, respectively.

B. Conflict Detection Network

The dataset for the training and evaluation of the detection network was collected during ground-walking trials, that is, the human subject wore the robot and walked by following a predefined trajectory under the fixed impedance model. The min-max normalization technique was also applied and used to reformat the sensory data and ensure they were on the same scale (see Fig. 5). When the human-robot interaction was going smoothly such that the human (wearing the exoskeleton) can follow the trajectory properly, the collected data was regarded as normal. Otherwise, it was labelled as abnormal, due to the physical conflicts between the human and the robot.

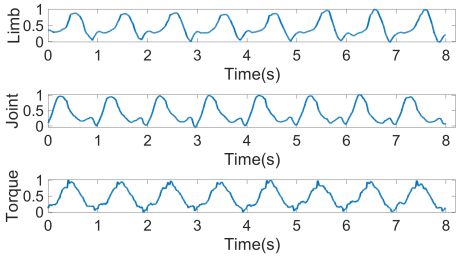

Fig. 5. Processed data from proprioceptive sensors, including the angle of human limb (top, measured with IMUs), the angle of robot joint (middle, measured with encoders), and the interaction torque (bottom, measured with encoders and known stiffness).

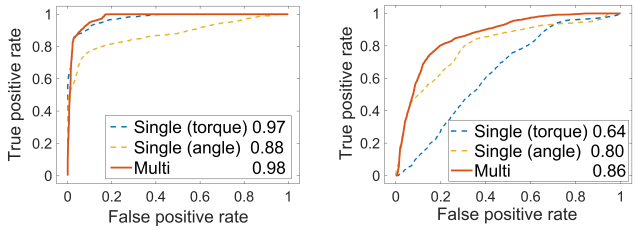

(a) (b)

Fig. 6. The AUC value (shown in the legend) and the ROC curve of multi-modal detection with respect to the single one (using the torque or the IMU information only): (a) the scenario of asynchronization; (b) the scenario of imbalance.

During the experiment, the human subject intentionally held the robot, which resulted in a simulated conflict, and the output of the detection network was shown in Fig. 7(a). As can be seen, the reconstruction error increased significantly when the conflict arose, proving the anomalous issue could be recognized and successfully separated. The performance of the detection network was also validated in another simulated conflict, where the human subject lost balance due to fatigue. The results are shown in Fig. 7(b), also proving the successful detection of such a conflict.

In addition, ablation studies were carried out to show that using the multi-modal information achieves more accurate detection compared to single sensory input; the comparison results are shown in Fig. 6. Note that the curve of receiver operating characteristic (ROC) was introduced to describe the detection performance, which implies how well a classification model can distinguish between classes; In general, a larger area under the curve (AUC) indicated a better performance, and vice versa. It can be seen from Fig. 6 that the multi-modal detection has a higher AUC than single sensory input in both scenarios (i.e., asynchronization and imbalance), that is, the proposed scheme with multi-modal information ensured more accurate detection. This was because the multi-modal information was able to handle different anomaly scenarios with specific manifestations. For example, in the presence of asynchronization between the human and robot, the interaction torque quickly increases. When an imbalance issue arises due to human fatigue, the angular information about the human limb, such as IMUs signals, would change more obviously.

C. Variable Impedance Control

Next, the proposed variable impedance controller, described by (11)-(13), was implemented in the exoskeleton robot, to enable the robot to assist the human while detecting and relaxing physical conflicts. The impedance parameters were set as: $\boldsymbol{C}_d = 15\boldsymbol{I}_4, \boldsymbol{K}_d = 13\boldsymbol{I}_4$ where $\boldsymbol{I}_4$ is an 4×4 identity matrix, and the parameters of the weighting function were set as: $\lambda_1 = 4.5, m = 0.02, h = 5.75, \lambda_2 = 5.5$, and the control parameters were set as: $\boldsymbol{K}_v = 10^{-3}\boldsymbol{I}_4, \boldsymbol{K}_z = 25\boldsymbol{I}_4$. The experimental results are shown in Fig. 8. It can be seen that the impedance parameters were scaled down (i.e., $w(s)$) when the anomaly score increased, relaxing the conflicts. The adjustment of impedance is continuous as the change of $w(s)$ is smooth, thereby ensuring safe human-robot interaction. The impedance vector $\boldsymbol{z}$ remained zero, proving the realization of the variable impedance model. The proposed variable impedance controller was also compared with a fixed impedance controller (by setting $w(s) = 10$), and the results were shown in Fig. 9, implying relaxing the conflict with the variable impedance was more comfortable for the wearer because the RMS of EMG signal was smaller.

VII. Conclusions

In this paper, a multi-modal learning scheme is proposed to detect the physical conflicts between the human and the exoskeleton robot, using only proprioceptive sensors. The proposed scheme has the advantage of low cost and ease of implementation, and the use of multi-modal information helps to explore semantic implication during the physical interaction, thereby improves the accuracy of conflict detection. In addition, the anomaly score, as the output of the detection network, is embedded into the variable impedance controller to continuously modulate robot impedance to relax the conflict. Experimental results on a lower-limb exoskeleton robot are presented, where the EMG data shows that the variable impedance control with conflict detection can improve the comfort of the human wearer. Future works will be denoted to other scenarios, e.g., climbing the staircase, walking down the slope, and sit-to-stand.

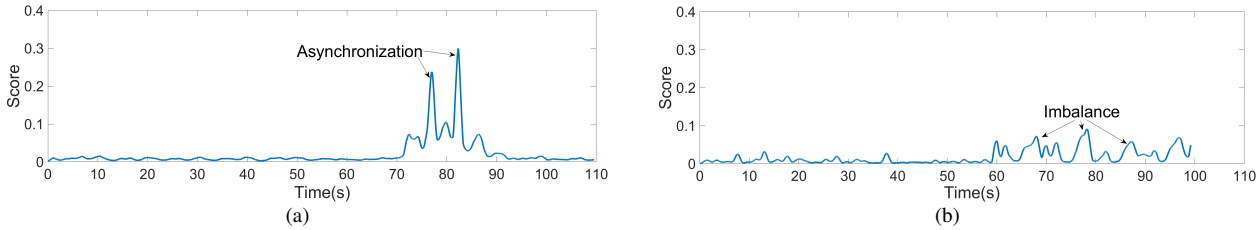

Fig. 7. Anomaly scores generated by the physical-detection network: (a) The human intentionally held the robot to simulate the asynchronization; (b) The imbalance issue arose due to human fatigue.

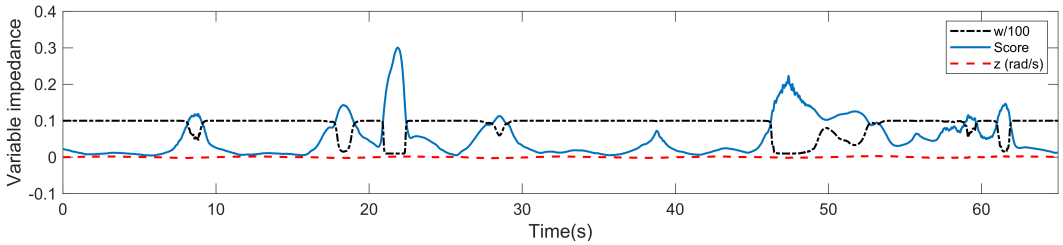

Fig. 8. Experimental results using the proposed variable impedance controller: The impedance parameters were scaled down (black dashed line) when the anomaly score increased (blue solid line), relaxing the conflicts; The adjustment of impedance is continuous as the change of $w(s)$ is smooth, ensuring the safe human-robot interaction; The impedance vector (red dashed line) remained zero, proving the realization of the variable impedance model.

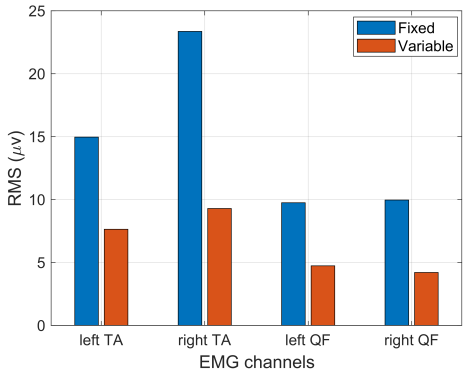

Fig. 9. Comparison results between the proposed variable impedance controller (red) and a fixed impedance controller (blue): Relaxing the conflict with the variable impedance makes the human more comfort, as the RMS of EMG signal is smaller.

APPENDIX

Substituting (11) into (2) yields

$$\boldsymbol{B}\ddot{\boldsymbol{\theta}} + \boldsymbol{K}(\boldsymbol{\theta} - \boldsymbol{q}) + \boldsymbol{K}_v(\dot{\boldsymbol{\theta}} - \dot{\boldsymbol{q}}) = \boldsymbol{u}_s, \tag{14}$$

which can be written as

$$\boldsymbol{B}(\ddot{\boldsymbol{\theta}} - \ddot{\boldsymbol{q}}) + \boldsymbol{K}(\boldsymbol{\theta} - \boldsymbol{q}) + \boldsymbol{K}_v(\dot{\boldsymbol{\theta}} - \dot{\boldsymbol{q}}) = \boldsymbol{u}_s - \boldsymbol{B}\ddot{\boldsymbol{q}}, \tag{15}$$

By introducing $\boldsymbol{\tau}_o = \boldsymbol{K}(\boldsymbol{\theta} - \boldsymbol{q})$, $\boldsymbol{K} = \boldsymbol{K}_1/\epsilon^2$ and $\boldsymbol{K}_v = \boldsymbol{K}_2/\epsilon$ with a small positive parameter ϵ, (1) and (15) can now be written as

$$\boldsymbol{M}(\boldsymbol{q})\ddot{\boldsymbol{q}} + \boldsymbol{C}(\dot{\boldsymbol{q}}, \boldsymbol{q})\dot{\boldsymbol{q}} + \boldsymbol{g}(\boldsymbol{q}) = \boldsymbol{\tau}_o + \boldsymbol{\tau}_e \tag{16}$$

$$\epsilon^2\boldsymbol{B}\ddot{\boldsymbol{\tau}}_o + \epsilon\boldsymbol{K}_2\dot{\boldsymbol{\tau}}_o + \boldsymbol{K}_1\boldsymbol{\tau}_o = \boldsymbol{K}_1(\boldsymbol{u}_s - \boldsymbol{B}\ddot{\boldsymbol{q}}). \tag{17}$$

which describes a singular perturbation problem. In condition of $\epsilon = 0$, the solution of (17) is obtained as $\bar{\boldsymbol{\tau}}_o = \boldsymbol{u}_s - \boldsymbol{B}\ddot{\boldsymbol{q}}$.

With the consideration of fast time-scale set as $\gamma = \frac{t}{\epsilon}$, $\bar{\boldsymbol{\tau}}_o$ is achieved at $\gamma \to \infty$. Note that $\bar{\boldsymbol{\tau}}_o$ remains constant at $\epsilon = 0$, a new variable is introduced as $\boldsymbol{\eta} = \boldsymbol{\tau}_o - \bar{\boldsymbol{\tau}}_o$ to rewrite (17) on fast time-scale:

$$\boldsymbol{B}(\frac{\mathrm{d}^2\boldsymbol{\eta}}{\mathrm{d}\gamma^2}) + \boldsymbol{K}_2(\frac{\mathrm{d}\boldsymbol{\eta}}{\mathrm{d}\gamma}) + \boldsymbol{K}_1\boldsymbol{\eta} = \boldsymbol{0}, \tag{18}$$

witch is referred to as *boundary-layer system*, and its the exponential stability can be guaranteed by appropriately tuning the parameters $\boldsymbol{K}_1$ and $\boldsymbol{K}_2$.

Then, substituting such a solution into (16), a *quasi-steady-state system* can be derived as

$$(\boldsymbol{M}(\boldsymbol{q}) + \boldsymbol{B})\ddot{\boldsymbol{q}} + \boldsymbol{C}(\dot{\boldsymbol{q}}, \boldsymbol{q})\dot{\boldsymbol{q}} + \boldsymbol{g}(\boldsymbol{q}) = \boldsymbol{u}_s + \boldsymbol{\tau}_e \tag{19}$$

Substituting (9) and (13) into (19) yields

$$(\boldsymbol{M}(\boldsymbol{q}) + \boldsymbol{B})\dot{\boldsymbol{z}} + \boldsymbol{C}(\dot{\boldsymbol{q}}, \boldsymbol{q})\boldsymbol{z} = -\boldsymbol{K}_z\boldsymbol{z}, \tag{20}$$

where $\hat{\boldsymbol{\tau}}_e \to \boldsymbol{\tau}_e$ by using the DOB.

Next, a Lyapunov-like candidate is proposed as

$$V = \boldsymbol{z}^T(\boldsymbol{M}(\boldsymbol{q}) + \boldsymbol{B})\boldsymbol{z}. \tag{21}$$

Differentiating (21) with respect to time and substituting (20) into it, we have

$$\dot{V} = -\boldsymbol{z}^T\boldsymbol{K}_z\boldsymbol{z}. \tag{22}$$

Since $V > 0$ and $\dot{V} < 0$, the *quasi-steady-state system* is also exponentially stable. According to Tikhonov's theorem [34], the stability of closed-loop system is guaranteed and the convergence to the impedance vector to zero is realized.

REFERENCES

[1] X. Li, X. Zhang, Xiu. Li, J. Long, G. Chen, and J. Ye. "BEAR-H: An Intelligent Bilateral Exoskeletal Assistive Robot for Smart Rehabilitation." *IEEE Robotics & Automation Magazine*, 2021.

[2] V. Grosu, C. R. Guerrero, B. Brackx, S. Grosu, B. Vanderborght and D. Lefeber, "Instrumenting complex exoskeletons for improved human-robot interaction," in *IEEE Instrumentation & Measurement Magazine*, vol. 18, no. 5, pp. 5-10, 2015.

[3] G. Aguirre-Ollinger and H. Yu, "Lower-Limb Exoskeleton With Variable-Structure Series Elastic Actuators: Phase-Synchronized Force Control for Gait Asymmetry Correction," in *IEEE Transactions on Robotics*, vol. 37, no. 3, pp. 763-779, 2021.

[4] A. Rodríguez-Fernández, J. Lobo-Prat, and J. M. Font-Llagunes. "Systematic review on wearable lower-limb exoskeletons for gait training in neuromuscular impairments." *Journal of neuroengineering and rehabilitation*, 2021.

[5] A. Cicchella, "Development of the biomechanical technologies for the modeling of major segments of the human body: linking the past with the present." *Biology*, 2020.

[6] F. Crenna, G. B. Rossi and M. Berardengo, "A Global Approach to Assessing Uncertainty in Biomechanical Inverse Dynamic Analysis: Mathematical Model and Experimental Validation," in *IEEE Transactions on Instrumentation and Measurement*, vol. 70, pp. 1-9, 2021.

[7] R. C. U. of Sydney, C. M. C. R. Centre, S. C. Q. C. R. Institute, and Hbku, "Deep learning for anomaly detection: A survey," 2019.

[8] G. Münz, S. Li, and G. Carle, "Traffic anomaly detection using k-means clustering," 2007.

[9] R. Kumari, Sheetanshu, M. K. Singh, R. Jha, and N. K. Singh, "Anomaly detection in network traffic using k-mean clustering," *2016 3rd International Conference on Recent Advances in Information Technology (RAIT)*, pp. 387–393, 2016.

[10] M. Yang and D. Ergu, "Anomaly detection of vehicle data based on lof algorithm," 2020.

[11] X. Xu, Y. Lei, and X. Zhou, "A lof-based method for abnormal segment detection in machinery condition monitoring," *2018 Prognostics and System Health Management Conference (PHM-Chongqing)*, pp. 125–128, 2018.

[12] Z. Gan and X. Zhou, "Abnormal network traffic detection based on improved lof algorithm," *2018 10th International Conference on Intelligent Human-Machine Systems and Cybernetics (IHMSC)*, vol. 1, pp. 142–145, 2018.

[13] D. J. Samuel and F. Cuzzolin, "Unsupervised anomaly detection for a smart autonomous robotic assistant surgeon (saras) using a deep residual autoencoder," *IEEE Robotics and Automation Letters*, vol. 6, pp. 7256–7261, 2021.

[14] P. Malhotra, L. Vig, G. M. Shroff, and P. Agarwal, "Long short term memory networks for anomaly detection in time series," in *ESANN*, 2015.

[15] D. Park, Y. Hoshi, and C. C. Kemp, "A multimodal anomaly detector for robot-assisted feeding using an lstm-based variational autoencoder," *IEEE Robotics and Automation Letters*, vol. 3, pp. 1544–1551, 2018.

[16] Y. Su, Y. Zhao, C. Niu, R. Liu, W. Sun, and D. Pei, "Robust anomaly detection for multivariate time series through stochastic recurrent neural network," *Proceedings of the 25th ACM SIGKDD International Conference on Knowledge Discovery & Data Mining*, 2019.

[17] L. Damm, and J. McIntyre, "Physiological basis of limb-impedance modulation during free and constrained movements." *Journal of neurophysiology* vol. 100, no. 1, pp. 2577-2588, 2008.

[18] M. Sharifi, A. Zakerimanesh, J. K. Mehr, A. Torabi, V. K. Mushahwar, M. Tavakoli, "Impedance variation and learning strategies in human-robot interaction." *IEEE Transactions on Cybernetics*, 2021.

[19] Y. Huo, X. Li, X. Zhang and D. Sun, "Intention-Driven Variable Impedance Control for Physical Human-Robot Interaction," *2021 IEEE/ASME International Conference on Advanced Intelligent Mechatronics (AIM)*, pp. 1220-1225, 2021.

[20] L. Rozo, S. Calinon, D. G. Caldwell, P. Jiménez and C. Torras, "Learning Physical Collaborative Robot Behaviors From Human Demonstrations," in *IEEE Transactions on Robotics*, vol. 32, no. 3, pp. 513-527, 2016.

[21] F. Ficuciello, L. Villani and B. Siciliano, "Variable Impedance Control of Redundant Manipulators for Intuitive Human–Robot Physical Interaction," in *IEEE Transactions on Robotics*, vol. 31, no. 4, pp. 850-863, 2015.

[22] Y.-C. Pai, B. E. Maki, K. Iqbal, W. E. McIlroy, and S. D. Perry, "Thresholds for step initiation induced by support-surface translation: a dynamic center-of-mass model provides much better prediction than a static model." *Journal of biomechanics*, vol. 33, no. 3, pp. 387–92, 2000.

[23] X. Zhang, L. Sun, Z. Kuang and M. Tomizuka, "Learning Variable Impedance Control via Inverse Reinforcement Learning for Force-Related Tasks," in *IEEE Robotics and Automation Letters*, vol. 6, no. 2, pp. 2225-2232, 2021.

[24] M. Bogdanovic, M. Khadiv and L. Righetti, "Learning Variable Impedance Control for Contact Sensitive Tasks," in *IEEE Robotics and Automation Letters*, vol. 5, no. 4, pp. 6129-6136, 2020.

[25] C. Yang, C. Zeng, C. Fang, W. He and Z. Li, "A DMPs-Based Framework for Robot Learning and Generalization of Humanlike Variable Impedance Skills," in *IEEE/ASME Transactions on Mechatronics*, vol. 23, no. 3, pp. 1193-1203, 2018.

[26] Z. Jin, A. Liu, W.-a. Zhang and L. Yu, "An Optimal Variable Impedance Control With Consideration of the Stability," in *IEEE Robotics and Automation Letters*, vol. 7, no. 2, pp. 1737-1744, 2022.

[27] C. C. Cheah and X. Li, *Task-space sensory feedback control of robot manipulators*. vol. 73. Springer, 2015.

[28] S. Arimoto, "Control theory of nonlinear mechanical systems," *A Passivity-based and Circuit-theoretic Approach*, 1996.

[29] M. M. Olsen and H. G. Petersen, "A new method for estimating parameters of a dynamic robot model," *IEEE Trans. Robotics Autom.*, vol. 17, pp. 95–100, 2001.

[30] D. P. Kingma, and M. Welling. "Auto-encoding variational bayes." arXiv preprint arXiv:1312.6114, 2013.

[31] C. A. Oatis, "The use of a mechanical model to describe the stiffness and damping characteristics of the knee joint in healthy adults." *Physical Therapy*, vol. 73, no. 11, pp. 740–749, 1993.

[32] A. Mohammadi, H. J. Marquez and M. Tavakoli, "Nonlinear Disturbance Observers: Design and Applications to Euler-Lagrange Systems," in *IEEE Control Systems Magazine*, 2017.

[33] H. K. Khalil, *Nonlinear Systems*, Macmillan Publishing Company, 1992.

[34] A. N. Tikhonov, "Systems of differential equations containing small parameters in the derivatives." *Matematicheskii sbornik*, vol. 73 ,pp. 575–586, 1952.